NASA Technical Memorandum 78614

Analysis of Coastal Upwelling and the Production of a Biomass

John T. Howe

November 1979

NASA

National Aeronautics and
Space Administration

Analysis of Coastal Upwelling and the Production of a Biomass

John T. Howe, Ames Research Center, Moffett Field, California

NASA

NOMENCLATURE

a	coefficient in velocity expression (eq. (8)), related to upwelling index
$\bar{\bar{a}}$	argument in confluent hypergeometric function related to eigenvalues, equation (A17)
A_p	coefficient in hypergeometric series, equation (A15)
c_i	mass concentration of biomass
c_{i_o}	value of biomass concentration at $x = \varepsilon$
c_N	nutrient concentration
c_p	specific heat of water
d	upwelled depth
f	Coriolis parameter defined by equation (6)
F	momentum flux divergence terms equations (2) and (3)
$_1F_1$	confluent hypergeometric functions, equation (A16)
g	gravitational constant, equation (4)
H	energy divergence term, equation (5)
J	species flux divergence term, equation (7)
k	eddy thermal conductivity of water
K_1, K_2	defined by equation (A2)
K_i	rate coefficient for production of biomass species i
n	argument in equation (A15) defined by equation (A14)
p	pressure
q_r	solar radiative flux
R	earth's radius
t	time
T	temperature
u	velocity component in the x direction

v	velocity component in the y direction
w	velocity component in the z direction
x,y,z	Cartesian coordinates and coordinates shown in figure 4
X, Z	defined by equation (A9)
α	coefficient of temperature in equation (4)
β	part of Coriolis function equation (6)
δ	defined in figure 3
$\varepsilon, \varepsilon'$	small distances in x
η	defined by equation (16)
θ_o	mean latitude of water mass of interest
λ	eigenvalues, equation (A10)
μ_ν	spectral absorption coefficient
ρ	water density
ϕ	defined by equation (A4)
ψ	defined by equation (A4)
ω_i	volumetric production rate
Ω	earth axial rotational vector component

Subscripts

i	species
N	nutrients
o	reference condition
p	pressure
r	radiative
x,y,z	partial derivatives with respect to
ν	spectral band

ANALYSIS OF COASTAL UPWELLING AND THE PRODUCTION OF A BIOMASS

John T. Howe

Ames Research Center

SUMMARY

An analysis is performed on coastal upwelling phenomena wherein the coastal upwelling index derived from weather data is used as input to a set of coupled differential equations that describe, in an approximate way, the fluid dynamics, radiative transfer in the sea, and the resulting production of a biomass. The curl of the wind stress vector is discussed in the context of the physical extent of the upwelling structure. An analogy between temperature and biomass concentration in the upwelled coastal water is derived and the relationship quantified. Theoretical results are discussed in the context of observed natural phenomena, remote satellite or airborne sensing to obtain biomass rate production coefficients, and aerospace technology utilization by the commercial fishing industry. The intent of the paper is to provide a relatively simple framework within which the dominant features of the problem are included. The paper is written in a manner which hopefully provokes scientific interest; but more importantly, is readable and provides useful insight to a vast user community of perceptive and extraordinary men and women who fish the seas.

INTRODUCTION

In the past decade, a great deal of attention has been given to the phenomena of coastal and oceanic upwelling (ref. 1), particularly along both coasts of North America, and to some extent the coastal water of South America and Africa. In the upwelling process, cold, nutrient, rich water is drawn from the depths to the ocean surface, where, typically, nitrates (NO_3) and phosphates (PO_4) and phytoplankton seed are exposed to sunlight in the euphotic zone. In this zone, the phytoplankton grow by uptake of the nutrients (ref. 2), and in turn are grazed upon by the zooplankton and anchoveta in a complicated biological process in which the phytoplankton are ultimately enriched by ammonium (NH_3) excreted by the zooplankton and the anchoveta. Because of the upwelling phenomena, these coastal regions are exceedingly productive in biomass and are particularly rich as a source of protein sought by fishing vessels of many nations. Other regions of the oceans are very productive fishing grounds as well, such as the shifting boundary of ocean circulations of the northern and southern hemispheres, locales near the Erben Sea mount (2400 km (1500 mi) west of the North American continent), and the Emperor Sea mount (about 1600 km (1000 mi) off the coast of Japan).

The coastal upwelling phenomena is caused by the Coriolis force that arises from the rotation of the earth, the configuration of the landmass, including bottom configuration, and is triggered by a wind of sufficient

strength and duration with a component parallel to the coast (refs. 3, 4) such that the surface water is driven offshore and is replaced by colder water drawn from the depths.

It has recently been reported (ref. 5) that such upwelling phenomena occur along the edge of the Arctic ice pack north of Spitzbergen, initiated by a strong wind blowing for a period of about 2 days. Similar phenomena may be partly associated with reports of extensive krill production in the Antarctic as well.

Although a great deal of effort has gone into ocean research over the past decade, there has been considerable criticism of a disciplinary approach, a lack of desired contribution to social goals, and a realization that much of marine science lies at some interface between conventional disciplines (ref. 6).

In the context of the present study, many disciplines are involved: fluid mechanics, radiative transfer, transport of and finite rate production and extinction of species, satellite (and perhaps airborne) technology, and a host of others. It is possible to focus on one discipline, such as fluid dynamics, to such a detailed extent that the interface with other disciplines cannot be described conveniently and in a way that relates to a prediction of the bio-mass production. The same may be said of the biological modeling or any other feature relevant to the end object.

Thus for present purposes, we make every reasonable simplification to arrive at some gross behavior of the system and examine what sorts of param-eters may be monitored on a global scale that would provide useful information to a user community. To the extent that the reader desires, additional details, refinements, and features of the problem may be added to the analysis that follows.

It is a pleasure to acknowledge the very helpful comments of Dr. Larry Breaker of the U.S. Department of Commerce, NOAA/NESS, and Mr. Robert C. Wrigley of NASA-Ames Research Center.

ANALYSIS

Figure 1 is an enlargement of a computer-enhanced photograph taken by a TIROS weather satellite,[1] which used infrared imagery to display the tempera-ture structure of the ocean along the California coast on July 10, 1976. Dark tones indicate warm water and light tones show coastal upwelling of relatively cold water that originated below the surface. The cold upwelled water pattern tends to follow bathymetric features, with fronts extending approximately to the edge of the continental shelf (48 km (30 mi) west of San Francisco) and closer to shore between Point Arena and Cape Blanco where the bottom

---

[1]Breaker, Larry: Private communication, NOAA/NESS Satellite Field Service Station, Redwood City, California, 1976.

configuration drops off sharply near shore. A long tongue of upwelled water emanates southwesterly from Point Arena, possibly initiated by the underwater ridge associated with that point. The tongue is carried southeasterly by the sluggish California current. It may also be noted that the waters of the San Francisco Bay system are warm (dark toned), and a warm thermal plume proceeds southerly from the Golden Gate Bridge, interrupting the pattern of cold upwelled water.

Such an upwelling pattern is established by a strong wind from the northwest, which typically persists periodically for perhaps 3 days at a time during the late winter, spring, and summer months. During such a blow, cloud cover disappears and enables a satellite photograph to be obtained. As the wind diminishes, the cloud cover tends to return, but the upwelling pattern tends to persist for a number of days until it is altered by another weather system. It should be noted that upwelling "weather" may be quite localized as it is influenced by headlands and other features (discussed subsequently). The author has fished off Pidgeon Point in winds and seas that posed an immediate health hazard, although a weather update reported light northwesterly winds of 10 to 20 knots and seas of 0.9 to 1.5 m (3 to 5 ft) from Point Arena to Point Pinos. A satellite, of course, can give a detailed panoramic map of the entire upwelling system. Usually, one or two such satellite upwelling pictures can be obtained every week, which is sufficient to guide fishing vessels to the strongest fronts. As the initial strong winds begin to diminish, commercial fishermen begin to venture forth from harbors in a sequence that depends on the seaworthiness of their vessels and their individual tolerance to physical abuse.

When the wind stops or changes direction, the upwelling will terminate. A typical event occurred on May 6, 1976 in Monterey Bay during a northwesterly wind of "small-craft-advisory" proportions. A satellite photograph revealed unusually strong upwelling in Monterey Bay, and commercial fish buyers in Monterey reported that their facilities were strained to process the very large catch of salmon. By May 11, the wind was light from the northeast, a satellite photograph revealed no upwelling in Monterey Bay, and at the end of the day, Monterey fish buyers reported to the author that no salmon had been marketed that day. That situation prevailed until May 14, when a small-craft-advisory wind from the northwest revived the upwelling and the fishery.

There has been an attempt to mark the boundaries of the upwelling regions on a mercator projection chart (fig. 2), which is distributed by Humboldt State University Marine Advisors (ref. 7) to 11 fishing ports in California. A typical chart is shown in figure 2, corresponding to the satellite photo of figure 1.

Some weak boundaries are delineated as well as stronger broad boundaries. Whether or not the boundaries are all "fronts" in the sense that the upwelling structure is a cell of water that turns downward at the outer boundary is not clear. This may be especially true near headlands because of the windshadow effect where the headland shelters the region downwind. Upwind of a headland, the wind curl (to be discussed subsequently) may be either positive or negative, corresponding to stronger or weaker winds offshore. The negative wind curl tends to form fronts while the positive wind curl tends to move cold

plumes of upwelled water farther offshore (and may produce long tongues of upwelled water near headlands). However, downwind of a headland, if the headland provides windshadow, the tendency is toward positive wind curl, and boundaries within the shadow may not produce "downwelling" fronts. However, if these boundaries extend beyond the windshadow, they may or may not produce frontal structure, depending on the sign of the offshore wind curl.

With respect to figure 1, the weaker "fronts," such as those near Point Arena, south, near the San Francisco Bay, and between Monterey Bay and Point Conception are "inshore" of stronger fronts. These weak fronts are often fished by large numbers of small commercial vessels as a matter of convenience and safety — the fronts are roughly 2 hr running distance, or 30 km (~19 mi), from port or shelter. Thus, 4 hr running time, or 60 km (~37 mi), are required for a day's fishing trip. However, productivity of these weak fronts is often marginal for the salmon fishery; the weak fronts yield relatively small numbers of smaller fish. However, the stronger coastal fronts, which may lie 90 km (~60 mi) offshore, tend to be more productive and are accessible to the same commercial fleet of small craft, if they know where to find the fronts. It is becoming increasingly necessary for them to do so to remain economically viable since increased regulation tends to restrict their catch, fuel costs rise, and fishing is restricted in both Mexican and Canadian waters. Thus, American coastal waters must be fished with greater efficiency for this fleet to maintain its utility. The cost is largely due to inconvenience, with 4 to 6 hr running time, or 60 to 90 km (~37 to 56 mi), each way and quite possibly one or more nights spent on the fishing grounds with the catch preserved in ice. For the most part, the stronger coastal fronts are accessible to the existing commercial fleet of small craft — typically 10 to 15 m (33 to 50 ft) in length (a representative vessel and its gear is shown in fig. 3). These generally carry modern electronics for communications and navigation — one or more two-way radios, radar, Loran, depth recorders and flashers, autopilots, and compasses. Moreover, they carry hydraulically operated fishing equipment, such as shown at the bottom of figure 3, and have a cruising range 1000 to 2000 km (621 to 1242 mi). Given the location of the strong fronts periodically, these numerous craft can fish them economically. For far-offshore fisheries mentioned previously, a fleet of larger, more sophisticated, seaworthy vessels is in operation, and can be aided by a knowledge of offshore fishery locations, improved weather information, and improved communications from satellite technology.

Mathematical Formulation

This section is presented primarily for those whose interest is in modeling upwelling structures mathematically. It is a point of reference for the analysis that follows. Those who are not familiar with the detailed set of hydrodynamic equations may wish to go directly to the next section where certain assumptions are made that greatly simplify the analysis, thus sacrificing precision in the hope of obtaining a glimpse of the gross features and parameters of the solution.

The general equations that describe the water motion (refs. 8 and 9) are statements of conservation of mass (eq. (1)), momentum (eqs. (2), (3), and (4)), and energy (eq. (5)):

$$\frac{\partial \rho}{\partial t} + \rho \frac{\partial u}{\partial x} + \rho \frac{\partial v}{\partial y} + \rho \frac{\partial w}{\partial z} = 0 \tag{1}$$

$$\frac{\partial u}{\partial t} + u \frac{\partial u}{\partial x} + v \frac{\partial u}{\partial y} + w \frac{\partial u}{\partial z} - F_1 - fv - \frac{1}{\rho} \frac{\partial p}{\partial x} = 0 \tag{2}$$

$$\frac{\partial v}{\partial t} + u \frac{\partial v}{\partial x} + v \frac{\partial v}{\partial y} + w \frac{\partial v}{\partial z} - F_2 + fu + \frac{1}{\rho} \frac{\partial p}{\partial y} = 0 \tag{3}$$

$$g(1 - \alpha T) + \frac{1}{\rho_0} \frac{\partial p}{\partial z} = 0 \tag{4}$$

$$\frac{\partial T}{\partial t} + u \frac{\partial T}{\partial x} + v \frac{\partial T}{\partial y} + w \frac{\partial T}{\partial z} - H = 0 \tag{5}$$

where the Coriolis parameter or latitude function is

$$f(y) = 2\Omega \left(\sin \theta_0 + \cos \theta_0 \frac{y}{R} \right) = f_0 + \beta y \tag{6}$$

and contains the effect of the rotation and curvature of the earth, and F and H are the momentum and energy flux divergence term. Here the usual approach of the oceanographer to large-scale phenomena has been adopted that uses pseudolaminar models involving constant transport coefficients as free parameters, and the z coordinate is directed upward in a "right-handed" coordinate system. In other formations (ref. 10, p. 433), the z coordinate is directed downward, a convention that will be adopted here, but retains a right-handed coordinate system. To these equations we add a species conservation equation

$$\frac{\partial c_i}{\partial t} + u \frac{\partial c_i}{\partial x} + v \frac{\partial c_i}{\partial y} + w \frac{\partial c_i}{\partial z} - J = \frac{\omega_i}{\rho} \tag{7}$$

where J is the species flux divergence term.

Approximate Solutions

In keeping with the remarks of the last two paragraphs of the introduction, we take the local upwelling process to be essentially two dimensional and idealize the geometry of the phenomena to the coordinate system shown in figure 4, where the upwelling region is considered to be rectangular for convenience, and the z coordinate is downward. The schematic shown in figure 4 omits the detailed structure of the Ekman velocity spiral for convenience, and net transport offshore is simply characterized by an offshore velocity u (ref. 11). Moreover, figure 4 shows a distinct frontal interface with the ocean. This is generally considered to be associated with negative wind stress curl near the front, which is conducive to "frontogenesis," and will be

5

mentioned subsequently. By contrast, positive wind stress curl tends to move coastal upwelled water farther offshore where it is mixed with, and diluted by, oceanic water. Moreover, for present purposes, we assume that the fluid dynamics has been established by a wind stress of sufficient duration and the upwelling is in the steady state and brings cold nutrient-rich water to the surface euphotic zone where it is warmed by sunlight and a plankton bloom occurs as the surface water moves offshore. Because these are the phenomena we wish to consider, we keep the fluid dynamics very simple. For reference purposes, the scales d and 2δ are of the order 200 m (660 ft) and 90 km (56 mi) (near Point Reyes, for example).

In figure 4, we might note that at the coordinate origins where x and z are zero, and again where the surface waters downwell at the "upwelling front" (x = 2δ), the flow resembles that of a stagnation point (ref. 12). Thus, if the alongshore current varies slowly with y locally, the flow is essentially two dimensional and the continuity equation (1) is satisfied by

$$u = ax \, , \qquad w = -az \qquad \text{for} \quad 0 \le x \le \delta \tag{8}$$

and

$$u = -a(x - 2\delta) \, , \qquad w = az \qquad \text{for} \quad \delta < x \le 2\delta \tag{9}$$

where a can be related to the upwelling index (refs. 3, 4) as follows. The upwelling index, I, is the component of Ekman transport directed offshore (refs. 3, 4). The Ekman transport is defined as

$$\vec{M} = \frac{1}{f} \vec{\tau} \times k \tag{10}$$

where k is a unit vector directed upward, f is the Coriolis parameter, and $\vec{\tau}$ is the sea surface shear stress vector resulting from the geostrophic wind and is described in references 3 and 4 as

$$\vec{\tau} = \rho_a c_D |\vec{U}| \vec{U} \tag{11}$$

where ρ_a is the density of the air, c_D is an empirical drag coefficient, and $\vec{U}$ is the wind vector near the sea surface. The shear stress can also be computed from boundary-layer theory of a wind blowing over a liquid surface, but the present formulation will suffice.

Thus, to the order of the depth of the well-mixed photosynthesis zone approximation, the quantity a can be related to the upwelling index I by

$$I = \rho u d_1 = ax\rho d_1 \tag{12}$$

where x should be evaluated at some reference point such as ε, and d_1 is the depth of the well-mixed layer in which photosynthesis takes place and is of the order of half a wavelength of the sea or swell. The dimensions of I are mass flux of water offshore per unit length of shoreline, in keeping with the terminology of references 3 and 4.

6

Thus, the component of the Ekman transport at the coastal boundary is related to the geostrophic wind at that boundary. In particular, the V component of the wind parallel to the coastal boundary, directed normal to the x, z plane of figure 4 (or down the coast), is of importance. As one moves offshore, the variation of that wind component becomes important. Thus, the curl of V, or $\partial V/\partial x$, is an important parameter, expecially if it is diminishing (negative) with distance offshore. When V becomes zero, one of the forces that drives the upwelling vanishes, and the upwelling structure tends to be arrested. Thus "a" in equation (8) is related to I at the coastal boundary; but the quantity "a" in equation (9) should probably be replaced by a quantity a', which is related to the negative curl of V. If the latter relationship were well known, the size (2δ) of the upwelling structure could be determined by matching the water velocity u at the juncture of the regions described by equations (8) and (9). The simplest relationship is to say that the upwelling structure terminates where V goes to zero. Although inertial or momentum considerations may preclude such simplicity, the relationship may be a useful estimate.

There have been many occasions when the author left port under very strong wind and sea conditions, wondering whether or not the ocean was fishable at all, only to find that the offshore environment was much more benign. Moreover, the front is often marked by a long line of Portuguese men-o-war, which would be blown away by any significant wind. This combination of weather conditions indicates a negative coastal wind curl, wherein the wind velocity becomes negligible at or near the front. In any event, the dimension of the upwelled region probably can be related to the wind curl in either an approximate or empirical manner. Such a relationship could probably be derived from remote sensing data or correlated from surface data. The effect of headlands can be determined as well. For present purposes, in a simple analytical framework in which to treat the entire problem, equations (8) and (9) are used to describe the flow field.

The energy equation may be written to include the energy flux divergence, $\rho c_p H$, explicitly as

$$\rho u c_p \frac{\partial T}{\partial x} + \rho w c_p \frac{\partial T}{\partial z} = \frac{\partial}{\partial z} \left(k \frac{\partial T}{\partial z} - q_{r_z} \right) \tag{13}$$

where k · is the "eddy conductivity," and q_{r_z} is the radiant flux at a depth

$$q_{r_z} = \sum_{\nu=1}^{\infty} q_{\nu_o} e^{-\mu_\nu z} \tag{14}$$

Here, q_{ν_o} is the spectral flux that penetrates the water. It has passed through the atmosphere, the air-sea interaction zone (ref. 13), and is the unreflected and unscattered residue of the incident flux that actually enters the water. A comparison of incident spectral solar radiation with the spectral extinction coefficients of seawater (refs. 11, 14) is shown in figure 5.

7

Generally, coastal water absorption is roughly double or triple that of oceanic water in the blue, green, yellow, and orange parts of the spectrum. Infrared radiation (wavelengths of about 1 μm or greater) is absorbed essentially on the water surface.

In equation (14), the diurnal variation of the spectral solar flux may be thought of as "properly averaged" or neglected. In any event, this detail, as well as others, can be added to a more precise analysis. For example, multiplying q_{ν_o} by a sinusoidal time function to simulate the diurnal radiation variation would not complicate the analysis excessively. Indeed, such a variation could produce results that lend credence to what some commercial fish trollers refer to as the "morning bite" and the "afternoon bite."

In equation (13) we neglect terms involving $\partial T/\partial z$ because energy absorbed from radiation is absorbed in surface layers (90% of incoming solar radiation is absorbed in the upper 10 m of the sea (refs. 15, 16)). The author has observed a Secchi disc disappear at depths ranging from as little as 0.67 to 5 m (~2.5 to 17 ft), at the most, in Northern California coastal waters. To the same order (10 m) the surface layers are "well stirred," say, to a depth of half a wavelength d_1 of the local sea or swell. Thus μ_ν in equation (14) is considered to be approximately constant, so that equations (13) and (14) become (averaged over the well-mixed layer)

$$\rho c_p a x \frac{\partial T}{\partial x} = -\sum_{\nu=1}^{\infty} \int_o^{d_1} \mu_\nu \cdot e^{-\mu_\nu z} q_{\nu_o} \frac{dz}{d_1} = \frac{1}{d_1} \sum_{\nu=1}^{\infty} q_{\nu_o} \tag{15}$$

with $\mu_\nu d_1 \gg 1$ assumed. Thus, for present purposes, the entire flux entering the water is absorbed.[2] For convenience, define

$$\eta = \frac{x}{\epsilon} \tag{16}$$

where ϵ is a convenient constant and could be related to the resolution of the remote temperature measurement for practical purposes. Thus, from equations (15) and (16)

$$\frac{d\eta}{\eta} = \frac{\rho c_p a d_1}{\displaystyle\sum_{\nu=1}^{\infty} q_{\nu_o}} dT \tag{17}$$

---

[2]This simple analysis could be embellished by including the Kubelka-Munk (ref. 17) equations to account for reflected light, and light that is backscattered in depth.

which integrates to

$$
T = \frac{\displaystyle\sum_{\nu=1}^{\infty} q_{\nu_0}}{\rho c_p a d_1} \, \ell n \, \eta + \text{constant} \tag{18}
$$

When $\eta = 1$, we define $T = T_0$ so that equation (18) becomes

$$
T - T_0 = \frac{\displaystyle\sum_{\nu=1}^{\infty} q_{\nu_0}}{\rho c_p a d_1} \, \ell n \, \eta \quad , \qquad 1 \leq \eta \leq \frac{\delta}{\varepsilon} \tag{19}
$$

Similarly, from equations (9) and (13) with the same approximations for $\delta/\varepsilon < \eta \leq 2(\delta/\varepsilon)$

$$
T - T_0 = \frac{\displaystyle\sum_{\nu=1}^{\infty} q_{\nu_0}}{\rho c_p a d_1} \, \ell n \left[\frac{\left(\frac{\delta}{\varepsilon}\right)^2}{2\left(\frac{\delta}{\varepsilon} - \eta\right)} \right] \tag{20}
$$

Figure 6 represents the corresponding surface temperature profile (left ordinate) for $\delta/\varepsilon = 500$, which is adequate for illustrative purposes. Because of the nature of the "stagnation"-type velocity distribution near the coast ($\eta = 0$) and near the extreme end of the upwelling structure ($\eta \sim 1000$), the residence time is large at those extremes and heating of the water is very significant compared to that in the intermediate region across the upwelling structure. It has been reported[3] that as one approaches the upwelling front (where the streamlines actually turn downward — fig. 4), the temperature may rise as much as 9.5 to 17°C. The ocean at the front is also experiencing a "stagnation"-type flow as it turns downward and is heated similarly (although to a lesser extent because of the lower absorption coefficients) so that a peak temperature occurs at the front and tapers off on both sides. This peak temperature, in effect, marks the offshore front. The asymptotic temperature approach to infinity at the front is a mathematical artifact resulting from the approximations made and is not physical. Thus, the solution should terminate at some distance, ε', before $x = 2\delta$, which could be determined from evaluation of the dimensionless ordinate and use of the limiting temperature rise cited above, or use of a measured or remotely sensed peak temperature. An alternate formulation of the energy equation that does not invoke some of the assumptions made, and leads to an analytic solution, is outlined in the appendix. The analytic solution is in terms of confluent hypergeometric functions, which may provide entertainment for 19th Century mathematicians, but adds little insight to the problem.

The "front" mentioned above is marked in other ways as well. Commercial fishermen often look for color change in the water to mark the front, and will declare that if they are within 16 km (~10 mi) of such a front, they will find it by watching water color (see fig. 5). The reason is that the upwelled

9

water is often green because of the nutrients and presence of a diffuse biomass, while the ocean water at the front tends to be blue because of a lack of these substances. Blue is the "desert" color of the sea. Another mark of the front is the flotsam and jetsome, which tend to be carried there by the sluggish current, where their offshore motion is arrested by the oceanic countercurrent that plunges downward at the front. Another means of identifying the front from shipboard is the presence of vast quantities of bait in the water near the front. As mentioned previously, the author has observed a line of Portuguese men-o-war as far as the eye could see along the front. These small creatures that float on the surface are incapable of swimming against the sluggish upwelled current, and in the absence of a strong wind, are simply carried to the front by the upwelled water, where they remain. While fishermen search for the front, so do the fish. For example, salmon in the euphotic zone are thought to have chemoceptors along the length of their body that detect biogradients. When the gradient peaks, they have found the front and tend to disperse throughout the water column along the front.

Consider now the production of species in the upwelled water. The greatest effect of sunlight on upwelled water is concerned with the metabolism of living organisms; it provides the energy for the photosynthetic processes of microscopic plantlife that all animals depend on for nourishment. The process has oxygen as a byproduct, which is of great importance to the respiration of animal organisms and in the oxidation of both organic and inorganic substances. The life cycle of any system of species is very complicated and in some cases can be modeled in a detailed way, such as that mentioned in the introduction. That particular model has been programmed by reference 2 in a manner that is weakly coupled to the physical world of fluid dynamics and radiative transfer as approximate boundary conditions for the biological model. The authors of reference 2 acknowledge that the "real world" is not adequately represented. Such a detailed biological model could be built into a more complete computer code that adequately simulates the fluid dynamics and spectral radiative transfer. Such a model would require rate coefficients for each step in the biological process.

It may be noted that the upwelling season lasts several months. Phytoplanckton tend to grow exponentially for, perhaps, 2 days, but then concentration levels off because of grazing by the zooplanckton, as they are carried offshore by the upwelled water. Thus for present purposes, we illustrate the biological process by simply using the previously mentioned fact that the photosynthetic process of species production ultimately depends on sunlight. Accordingly, we assume that the nutrient concentration is essentially invariant with x, and is well mixed in the z direction so that ω_i, the local production rate of biomass per unit volume, is proportional to the nutrient concentration c_N and divergence of the particular spectral band q_{ν_i} (or bands) of

flux that produces the energy to create a biomass concentration c_i. Thus, equation (7) becomes simply (in the quasi-steady state)

$$\rho u \frac{\partial c_i}{\partial x} = \omega_i \tag{21}$$

10

where the production rate per unit volume is

$$\omega_i = -K_i c_N \frac{\partial q_{v_i}}{\partial z} \tag{22}$$

The biomass concentration c_i typifies that which may be inferred from satellite imagery. Use of equations (8), (16), (21), and (22) in equation (2) yields, with the vertical averaging that produced equation (17)

$$\frac{a \rho d_1}{K_i c_N q_{v_{i_o}}} \frac{dc_i}{} = \frac{d\eta}{\eta} \tag{23}$$

which yields, as before

$$c_i - c_{i_o} = \frac{K_i c_N q_{v_{i_o}}}{a \rho d_1} \ell n \, \eta \, , \qquad 1 \le \eta \le \frac{\delta}{\varepsilon} \tag{24}$$

and

$$c_i - c_{i_o} = \frac{K_i c_N q_{v_{i_o}}}{a \rho d_1} \ell n \left[\frac{\left(\frac{\delta}{\varepsilon}\right)^2}{2\left(\frac{\delta}{\varepsilon} - \eta\right)} \right] , \qquad \frac{\delta}{\varepsilon} < \eta \le 2\left(\frac{\delta}{\varepsilon}\right) \tag{25}$$

which are identical in form to equations (19) and (20) and thus are represented by figure 6 (the right-hand ordinate).[4]

It should be noted that for both ordinates, in accordance with our well-mixed assumption, water temperature and biomass concentration are invariant with the depth z in the surface layers. The temperature insensitivity to depth z for small values of z has been verified experimentally by the author, while at sea, by his thermometer readings.

With reference to figure 6, the right-hand ordinate for biomass concentration in the upwelled waters, the biomass increases greatly near the upwelled front because of the increased residence time mentioned previously. On the oceanic side of the front, there is no biomass — unlike the continuous temperature behavior across the front that was caused by solar heating on both sides of the front as noted previously.

Rather, the high concentration of biomass on the upwelled side of the front is simply carried downward at the front. Three important conclusions

---

[4]An alternate treatment of the species equation, in which additional terms are retained, can be formulated like that of the energy equation, and would appear much like that outlined in the appendix.

may be made. First, the greatest concentration of surface biomass occurs at the front in the upwelled water. This is the place where bait abound and large fish feed. It is, of course, the best place to fish. Second, as the upwelled front plunges downward, it carries the large biomass with it so that the entire water column along the front also is well supplied. The author has found, by commercially fishing the entire water column along the front, that the salmon harvest in the upper and middle waters along the front is enormously superior in size and number to that away from the front; and that bottom fish along the front are also larger and greater in number. Third, within the approximations made, the dimensionless temperature profile is identical to the dimensionless biomass concentration profile, as shown in figure 6. The validity of this result could be tested by methods described in reference 15 in which water temperature and phytoplankton concentrations are sensed at wavelengths of 0.443 µm, referenced to 0.525 µm. Such measurements could yield absolute values for T_o and Ci_o as well. The analogy between temperature and biomass concentration leads to the relation (eqs. (19), (20), (24), and (25))

$$\frac{\left(c_i - c_{i_o}\right)}{\left(T - T_o\right)} = c_p K_i c_N \frac{q_{v_{i_o}}}{\sum\limits_{v=1}^{\infty} q_{v_o}} \tag{26}$$

Thus, the ratio of the biomass concentration increase to the temperature increase across the upwelling structure is proportional to the ratio of energy absorbed by photosynthesis to the total energy absorbed in the water mass.

CONCLUDING REMARKS

The simplified, analytic mathematical model of an upwelling front that has been presented is illustrative of the kind of mathematical study that could be done in greater detail by the use of computers. The detailed model could include more refined fluid dynamics, radiative transfer, and biological modeling, as well as an improved understanding of the actual wind curl and the effect of headlands on the wind curl. It could include a broad geographical region (even global) in an efficient way by dividing the region into appropriate sectors and using a parallel processing computer such as the ILLIAC IV. The computations could be made on a continuing basis, making use of satellite or airborne sensor data to predict biomass distribution and to achieve a better understanding of the mechanisms and the kinetic rate parameters of biomass production. The model could reduce the fuel consumption per unit mass of protein harvested and increase the protein harvest from the sea. It could discover new, untapped fisheries to harvest. It may reveal upwelled regions deficient in nutrients, into which nutrients could be air dropped to enhance productivity;[5] the technology exists to air drop up to 23 m[3] (6000 gal) per hour.

---

[5]Private communication from C. K. Lombard, Pacific Design, Inc., Palo Alto, California, 1979.

Moreover, as Ocean Thermal Energy Conversion (OTEC) activities increase (especially in areas where conventional fuels are not plentiful), the use of satellites, airborne surveys, and computer simulation of the effects of the physical and biological processes associated with an OTEC plant could be determined. To a first order, an OTEC plant discharge could be modeled as an axisymmetric upwelling that is not dependent on a wind parallel to the shore, but which produces a biomass and a fishery. When the OTEC plant is cleaned of biofouling, discharges will affect the biomass. These effects can be determined as discussed above, and the rate coefficients for the recovery or normalization of the biomass can be inferred by the same procedure.

Other uses of multidisciplinary aerospace technology on global problems suggest themselves: coastal zone monitoring and management; shoreline erosion, monitoring, and protection assessment; the seasonal beach sand distribution and budget, including the effect of river dams on shorelines; and the effects of artificial reefs and barriers on both the biomass and shoreline protection.

APPENDIX A

ALTERNATE FORMULATION OF THE ENERGY EQUATION

From equations (8), (13) and (14) the energy equation becomes

$$\rho c_p a x \frac{\partial T}{\partial x} - \rho c_p a z \frac{\partial T}{\partial z} = \frac{\partial}{\partial z}\left(k \frac{\partial T}{\partial z} - \sum_{\nu=1}^{\infty} q_{\nu_0} e^{-\mu_\nu z}\right) \tag{A1}$$

For constant k, let

$$K_1 = \frac{k}{a\rho c_p} \quad \text{and} \quad K_2 = \frac{1}{a\rho c_p} \tag{A2}$$

so that equation (A1) becomes

$$x \frac{\partial T}{\partial x} = K_1 \frac{\partial^2 T}{\partial z^2} + z \frac{\partial T}{\partial z} + K_2 \sum_{\nu=1}^{\infty} \mu_\nu q_{\nu_0} e^{-\mu_\nu z} \tag{A3}$$

let

$$T(x,z) = \phi(x,z) + \psi(z) \tag{A4}$$

The partial derivatives are then

$$T_x = \phi_x , \qquad T_z = \phi_z + \psi_z , \qquad T_{zz} = \phi_{zz} + \psi_{zz} \tag{A5}$$

$$x\phi_x = K_1(\phi_{zz} + \psi_{zz}) + z(\phi_z + \psi_z) + K_2 \sum_{\nu=1}^{\infty} \mu_\nu q_{\nu_0} e^{-\mu_\nu z} \tag{A6}$$

which is now split into two equations

$$x\phi_x = K_1\phi_{zz} + z\phi_z \tag{A7}$$

and

$$K_1\psi_{zz} + y\psi_z = K_2 \sum_{\nu=1}^{\infty} \mu_\nu q_{\nu_0} e^{-\mu_\nu z} \tag{A8}$$

Let

$$\phi(x,z) = X(x) \cdot Z(z) \tag{A9}$$

14

so that equation (A7) becomes

$$\frac{xX'}{X} = \frac{K_1 Z''}{Z} + \frac{zZ'}{Z} = \lambda^2 \tag{A10}$$

where the primes refer to ordinary derivatives and λ^2 is a set of constant eigenvalues so that

$$xX' - \lambda^2 X = 0 \tag{A11}$$

and

$$K_1 Z'' + zZ' - \lambda^2 Z = 0 \tag{A12}$$

The solution of equation (A11) is

$$X = x^{\lambda^2} \tag{A13}$$

while that of (A12) is

$$Z(z) = \omega(n) \tag{A14}$$

where $\omega(n)$ is a pair of confluent hypergeometric functions, the first of which is given by the series

$$\left.\begin{array}{c} \omega_1 = {}_1F_1\left(\bar{\bar{a}}, \frac{1}{2}, n\right) = \displaystyle\sum_{p=0}^{\infty} A_p n^p \\[4mm] A_p = \dfrac{\bar{\bar{a}}(\bar{\bar{a}}+1) \ \cdots \ (\bar{\bar{a}} + p - 1)}{\dfrac{1}{2}\left(\dfrac{1}{2} + 1\right) \ \cdots \ \left(\dfrac{1}{2} + p - 1\right)p!} \end{array}\right\} \tag{A15}$$

while the second is

$$\omega_2 = n^{1/2}{}_1F_1\left(1 + \bar{\bar{a}} - \frac{1}{2}, \ 2 - \frac{1}{2} \ ; \ n\right) \tag{A16}$$

and the second series of ${}_1F_1$ is like the first with $[1 + \bar{\bar{a}} - (1/2)]$, $[2 - (1/2)]$ in place of $\bar{\bar{a}}, 1/2$, respectively, where

$$\bar{\bar{a}} = \frac{\lambda^2}{2} \tag{A17}$$

includes the eigenvalues.

Equation (A8) can be solved by standard procedures; boundary conditions must be worked into the solutions of equations (A8), (A11), and (A12) in a tractable manner, and the eigenvalues must be determined. Evaluating the solution of equation (A1) in the manner outlined may prove to be tedious.

15

REFERENCES

1. O'Brien, J. J.:   An Annotated Bibliography Related to Oceanic Upwelling. Florida State University, ONR Contract N0014-67-A-0235-0002, 1977.

2. Walsh, J. J.; and Bass, P. B.:   Upwelling Biome 1:   Oceans — A Seagoing Simulation Program.   Special Rep. no. 48, Department of Oceanography, University of Washington, Seattle, 1971.

3. Bakhun, A.:   Daily and Weekly Upwelling Indices, West Coast of North America 1967-1973.   NOAA Tech. Rep. NMFS-SSRF-693, August, 1975.

4. Bakhun, A.:   Coastal Upwelling Indices, West Coast of North America 1946-1971.   NOAA Tech. Rep. NMFS-SSRF-671, 1973.

5. Buckley, T. G.; Gammelsrod, T.; Johannessen, O. M.; and Roed, L. P.:   Oceanic Structure at the Edge of the Arctic Ice Pack in Winter. Science, vol. 203, no. 4376, pp. 165-167, 1979.

6. Botzum, J. (Ed.):   Ocean Science News, vol. 21, no. 2, January 8, 1979.

7. Wyatt, B.; Dewees, C.; Thompson, T.; Richards, J.; and Jurick, K.:   Using Satellite Photos to Locate Temperature Fronts.   University of California Cooperative Extension, California Sea Grant Marine Advisory Publication, Marine Briefs #13, 1976.

8. Theoretical Hydrodynamics, L. M. Milne - Thomson, Fifth Edition, The MacMillan Co., New York, N.Y., pp. 78-80, 1968.

9. Oceanography, Robinson; A. R., Research Frontiers in Fluid Dynamics, Seeger and Temple Eds., pp. 507-508, 1965.

10. Sverdrup, Johnson and Fleming: The Oceans, Prentice Hall, Inc., 1942, pp. 80-89.

11. Duxbury, A. C.:   The Earth and Its Oceans, Addison Wesley, 1971, p. 216.

12. Schlichting, H.:   Boundary Layer Theory, 6th Edition, McGraw Hill Book Co., 1968, p. 88.

13. Schotland, R. M.:   Radiative Flux Crossing the Air-Sea Boundary, New York University Supplement, 1968, pp. 19-41.

14. Arvesin, J. C.; Millard, J. P.; and Weaver, E. C.:   Remote Sensing of Chlorophyll and Temperature in Marine and Fresh Waters, Astronautica Acta, Pergamon Press, 1973, pp. 229-239.

15. Jerlov, N. G.:   Optical Oceanography, Elsevier Publishing Co., 1968, pp. 3, 51, 58, 59.

16. McLellan: Elements of Physical Oceanography, Pergamon Press, 1965,
        p. 125.

17. Kubelka, P.; and Munk, R.: Zeitshrift fur Technische Physik, vol. 12,
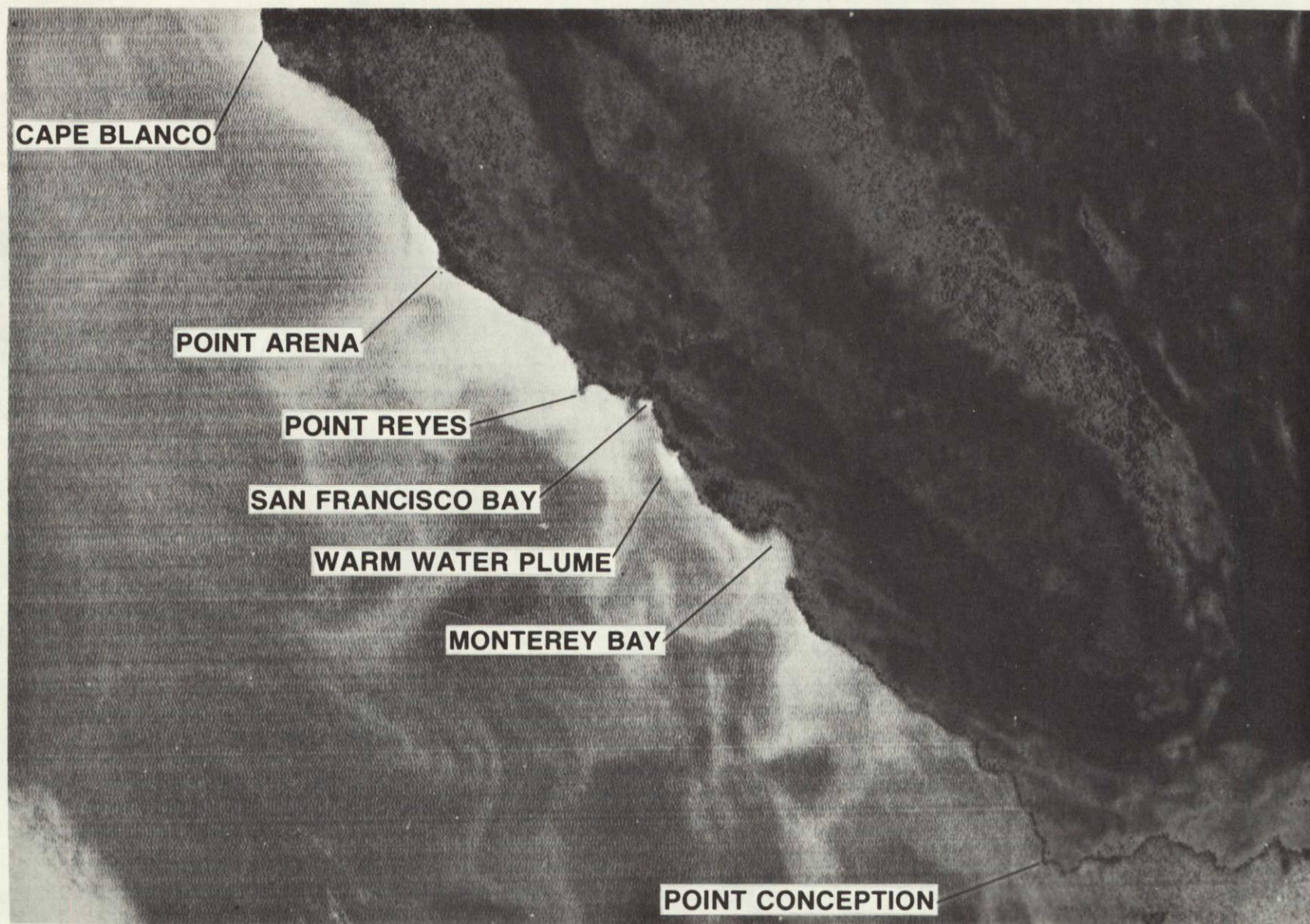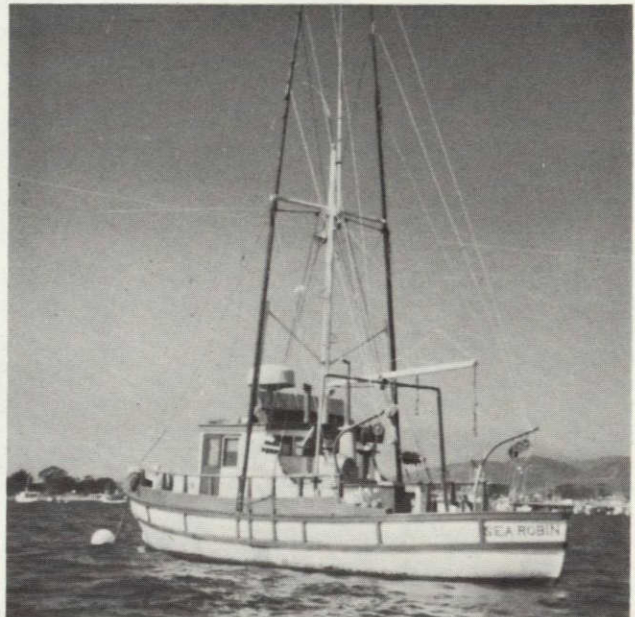   1931, p. 593.

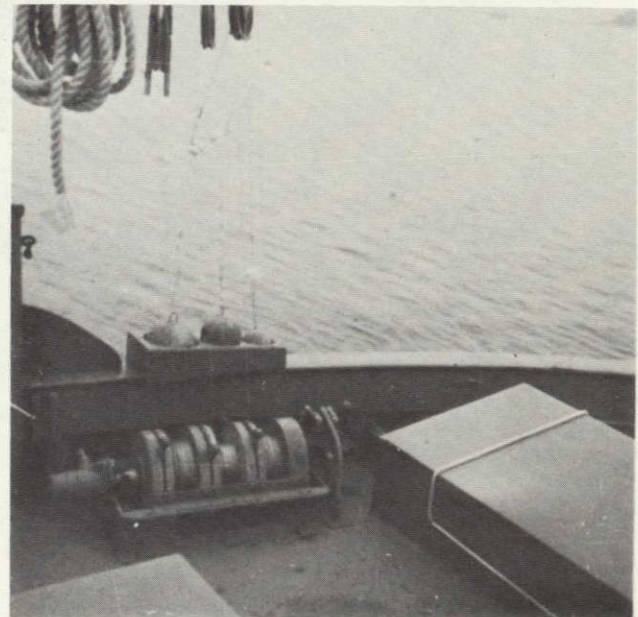Figure 1.- Central California coast showing upwelling, July 10, 1976.

18

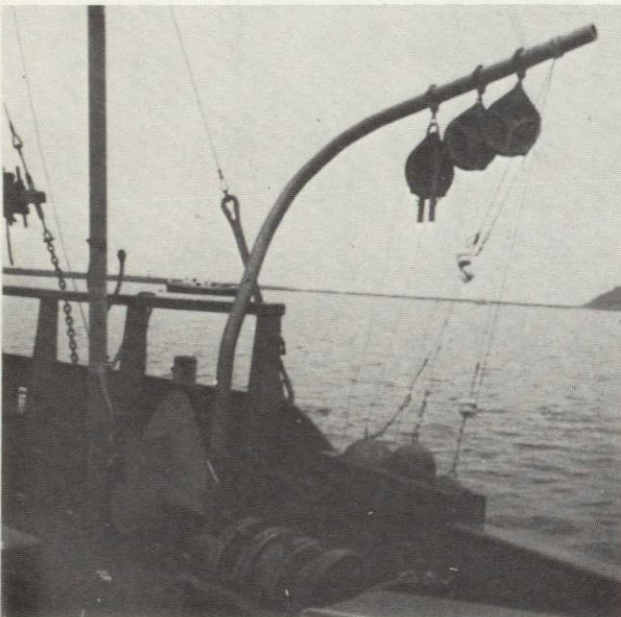Figure 2.- Mercator chart of upwelling fronts.

TYPICAL COASTAL FISHING CRAFT

HYDRAULIC FISHING GEAR

Figure 3.– Typical coastal commercial fishing vessel and its gear.

20

TYPICAL TEMPERATURE
PROFILE AT "UPWELLING FRONT"

SOLAR RADIATION

OCEANIC

ZONE

UPWELLING ZONE

COASTLINE

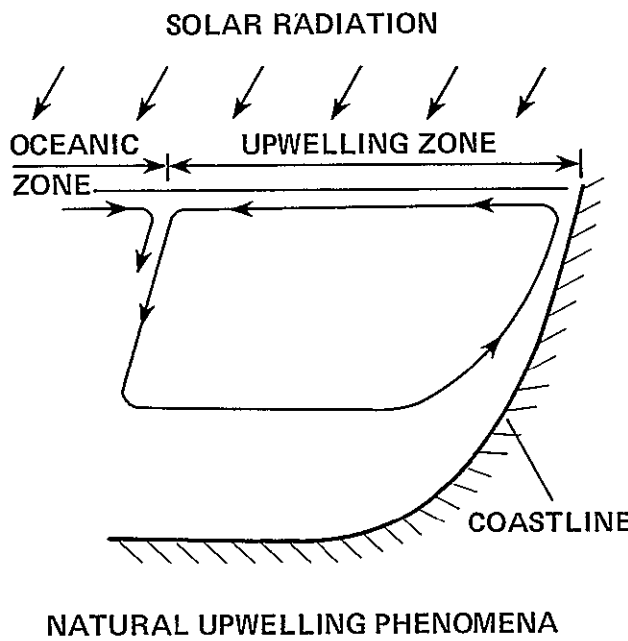NATURAL UPWELLING PHENOMENA

UPWELLING MODEL COORDINATES
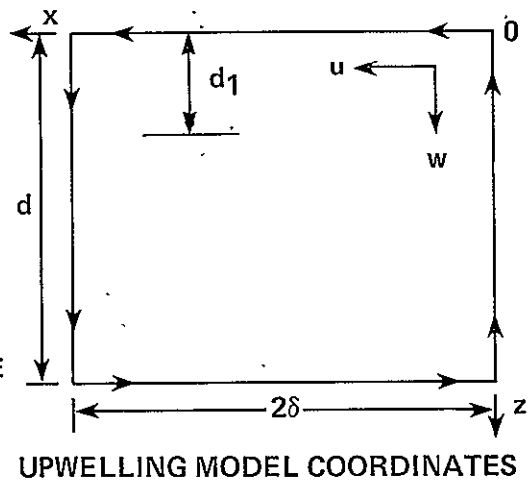
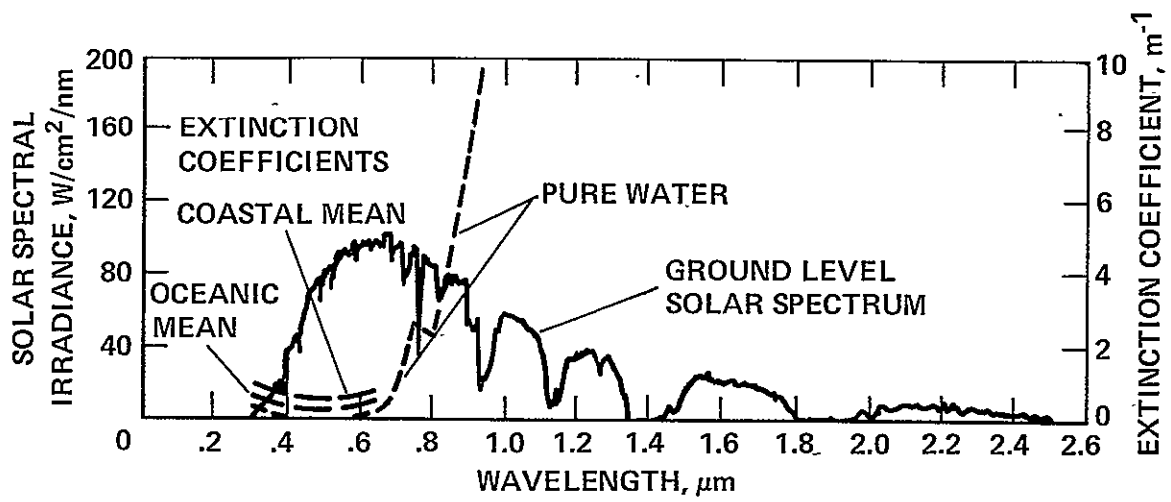Figure 4.- Physical model simulation.

21

Figure 5.- Comparison of solar spectrum with optical properties of water.
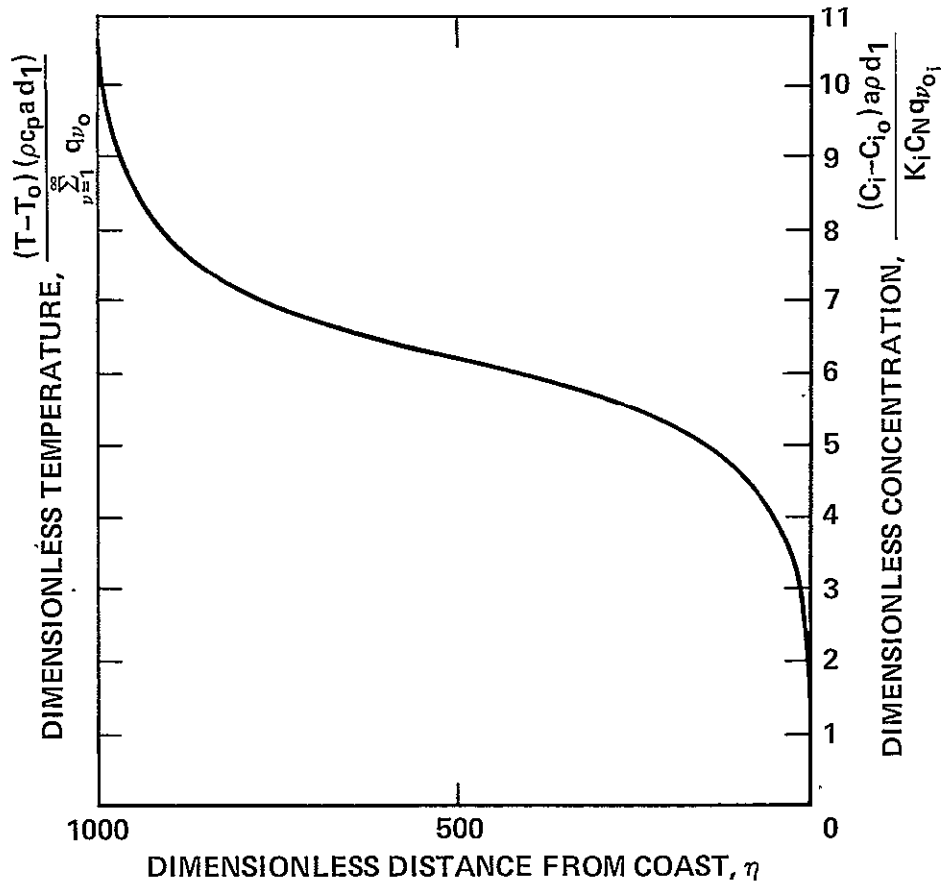
$$\delta/\epsilon = 500$$

Figure 6.— Normalized surface profiles for upwelling zone.

23

1. Report No. NASA TM-78614	2. Government Accession No	3. Recipient's Catalog No
4 Title and Subtitle ANALYSIS OF COASTAL UPWELLING AND THE PRODUCTION OF A BIOMASS		5. Report Date
		6. Performing Organization Code
7. Author(s) John T. Howe		8. Performing Organization Report No. A-7931
9. Performing Organization Name and Address Ames Research Center, NASA Moffett Field, Calif. 94035		10 Work Unit No. 506-26-21
		11. Contract or Grant No.
12. Sponsoring Agency Name and Address National Aeronautics and Space Administration Washington, D.C. 20546		13 Type of Report and Period Covered Technical Memorandum
		14 Sponsoring Agency Code

15. Supplementary Notes

16 Abstract

   An analysis is performed on coastal upwelling phenomena wherein the coastal upwelling index derived from weather data is used as input to a set of coupled differential equations that describe, in an approximate way, the fluid dynamics, radiative transfer in the sea, and the resulting production of a biomass. The curl of the wind stress vector is discussed in the context of the physical extent of the upwelling structure. An analogy between temperature and biomass concentration in the upwelled coastal water is derived and the relationship quantified. Theoretical results are discussed in the context of observed natural phenomena, remote satellite or airborne sensing to obtain biomass rate production coefficients, and aerospace technology utilization by the commercial fishing industry. The intent of the paper is to provide a relatively simple framework within which the dominant features of the problem are included. The paper is written in a manner which hopefully provokes scientific interest; but more importantly, is readable and provides useful insight to a vast user community of perceptive and extraordinary men and women who fish the seas.

17. Key Words (Suggested by Author(s)) Coastal upwelling Biomass Remote sensing	18 Distribution Statement Unlimited STAR Category - 48		
19. Security Classif. (of this report) Unclassified	20. Security Classif. (of this page) Unclassified	21. No. of Pages 27	22. Price* $4.50